Review

Not peer-reviewed version

Revisited Catalytic Hydrogen Evolution Reaction mechanism of MoS2

Yuhao He , Xiangpeng Chen , Yunchao Lei , Yongqi Liu , Longlu Wang *

Posted Date: 17 August 2023

doi: 10.20944/preprints202308.1283.v1

Keywords: catalytic mechanism; edge engineering; defect engineering; phase engineering

Review

Revisited Catalytic Hydrogen Evolution Reaction Mechanism of MoS_2

Yuhao He, Xiangpeng Chen, Yunchao Lei, Yongqi Liu and Longlu Wang *

College of Electronic and Optical Engineering & College of Flexible Electronics (Future Technology), Nanjing University of Posts and Telecommunications, Nanjing 210023, China

* Correspondence: wanglonglu@njupt.edu.cn

Abstract: MoS_2 has long been considered as a promising catalyst for hydrogen production. At present, there are many strategies to further improve its catalytic performance, such as edge engineering, defect engineering, phase engineering and so on. However, at present, there is still a great deal of controversy about the mechanism of MoS_2 catalytic hydrogen production. For example, it is generally believed that the base plane of MoS_2 is inert, but it has been reported that the inert base plane can undergo a transient phase transition in the catalytic process to play the catalytic role, which is contrary to the common understanding that the catalytic activity is only at the edge. Therefore, it is necessary to further understand the mechanism of MoS_2 catalytic hydrogen production. In this article, we summarized the latest research progress on the catalytic hydrogen production of MoS_2, which is of great significance for revisited the mechanism of MoS_2 catalytic hydrogen production.

Keywords: catalytic mechanism; edge engineering; defect engineering; phase engineering

1. Introduction

Hydrogen energy is the ultimate environment-friendly energy and the most promising form of energy to replace traditional energy sources such as coal, oil and natural gas [1–5]. At present, the production of hydrogen mainly relies on the cracking of traditional energy sources, which belongs to false decarbonization [6–8]. Hydrogen production by solar photovoltaic power generation is the most promising way of hydrogen production [9,10]. The key of electrocatalytic hydrogen production lies in the development and utilization of electrocatalyst. Although the precious metal platinum has good catalytic hydrogen production performance, it is the best hydrogen production catalyst at present, but its high cost and scarce resources seriously hinder its application in catalytic production.

As a non-precious metal catalyst with the most potential to replace precious metal platinum, MoS_2 has attracted more and more attention [11–16]. The key factors that determine the catalytic hydrogen production performance of MoS_2 are mainly two aspects, one is the number of active sites, and the other is the true activity of the active site [17–22]. It is generally believed that the base surface of MoS_2 is chemically inert and does not have the performance of catalytic hydrogen production, and at the same time, the edge of MoS_2 has a high catalytic hydrogen evolution activity [23–27]. More and more people are using various methods to expose the edge of MoS_2 to improve its catalytic hydrogen production performance [28–32]. The latest research shows that the conversion of sheet MoS_2 into bands can expose the edge sites and improve the catalytic hydrogen production performance [33–41]. It is also possible to directly generate branchlike MoS_2 by controlling the proportion of precursors during the growth of MoS_2, thereby increasing the edge site of MoS_2 [42–48]. Defect engineering and phase engineering are also strategies to regulate the catalytic hydrogen production performance of MoS_2 [49–56]. Although the catalytic hydrogen production performance of MoS_2 can be adjusted through various regulatory strategies, the corresponding catalytic mechanism is still very controversial. It has been reported that the inert base plane can undergo a transient phase transition in the catalytic process to play the catalytic role, which is contrary to the common understanding that the catalytic activity is only at the edge [57].

Only a deep and correct understanding of the catalytic mechanism of MoS_2 can further promote the design of high-performance MoS_2 structures, so as to promote the improvement of its catalytic

 doi:10.20944/preprints202308.1283.v1

performance. With the help of first principles theoretical calculation and in situ characterization, the catalytic process can be understood from the molecular and atomic levels and the mechanism of catalytic hydrogen production can be revealed. In this review, we introduce the latest research progress of strategies to improve the performance of MoS_2 catalytic hydrogen production, and give prospects for the development and direction of this research field.

2. Edge

It is well known that the edge site of MoS_2 has a high catalytic HER activity, and a lot of research has focused on how to expose the edge of MoS_2. Recent studies have shown that the MoS_2 can be designed with a rich edge structure such as a paired edge nanoribbon, which can further enhance the catalytic HER activity of MoS_2.

2.1. Nanoribbon

According to the research of edge-dominated electrochemical reaction kinetics in ultra-narrow MoS_2 nanoribbons, ideal energetics for HER could be obtained. Large arrays of MoS_2 nanoribbons were acquired by a templated subtractive patterning process (TSPP), which significantly enhance the turn-over frequency, exchange current density and lower the Tafel slope because of improved charge transfer efficiency.

Utilizing the naturally occurring bilayer and multilayer regions in graphene and taking advantage of the bottom-up approach of graphene, the pattern is transferred from the graphene mask to the surface of the MoS_2 material through a pattern transfer process, thus forming an aligned MoS_2 nanoribbon array with controlled direction as shown in Figure 1a. Since the formation of nanoribbons is random to a certain extent, the width distribution is also affected in Figure 1b. With a length-to-width ratio of more than 7,000 and a high density (Figure 1c), the strips are more efficient than other strategies for patterning MoS_2 nanoribbons. The observation of a single nanoribbon over a long distance in Figure 1d shows that the fractures are solved and the structural stability of the nanoribbon is ensured. By electron diffraction technique, the crystal properties of MoS_2 nanoribbons can be determined and characterized. The six-fold symmetry diffraction pattern in Figure 1e is observed in SAED model. Through the analysis of multiple SAED patterns of Figure 1f, the orientation of the nanoribbon will not affect the crystal structure. The atomic arrangement in the TEM of Figure 1g shows an orderly structure with no obvious defects. The difference in brightness may be due to the atomic number of the atoms, the darker atoms are Mo and the brighter are S. High basal plane quality makes their nanoribbon array an ideal model system for studying the source of HER enhancement. A three-electrode localized electrochemical microcell technique was employed to conduct electrochemical research. Consisting of an exposed reaction window and gold contact, as shown in the schematic of the microelectrode structure in Figure 1h and i, it may be used to place droplets for electrochemical studies. As shown in Figure 1j, the HER exchange current of MoS_2 nanoribbon arrays is significantly larger than that of pristine flakes and the overpotential has a decrease of 41%, which reveals an improved HER thermodynamic performance. Because the device is not deposited on a conductive surface and the carrier passes laterally through the nanoribbons from the electrode, introducing an uncompensated resistance, HER kinetics is quantified with the fitted Tafel curve. Tafel slope of the pristine flake is consistent with previous result, as a comparison, nanoribbon arrays' Tafel slope in Figure 1k has greatly decreased, showing the impact of edges on the improved HER kinetics of MoS_2. It can also point out that the observed Tafel slope is in good agreement with prior findings on edge enriched 2D materials, and it exhibits a clear distinction from alternative functionalization approaches.

Preprints (www.preprints.org) | NOT PEER-REVIEWED | Posted: 17 August 2023 doi:10.20944/preprints202308.1283.v1

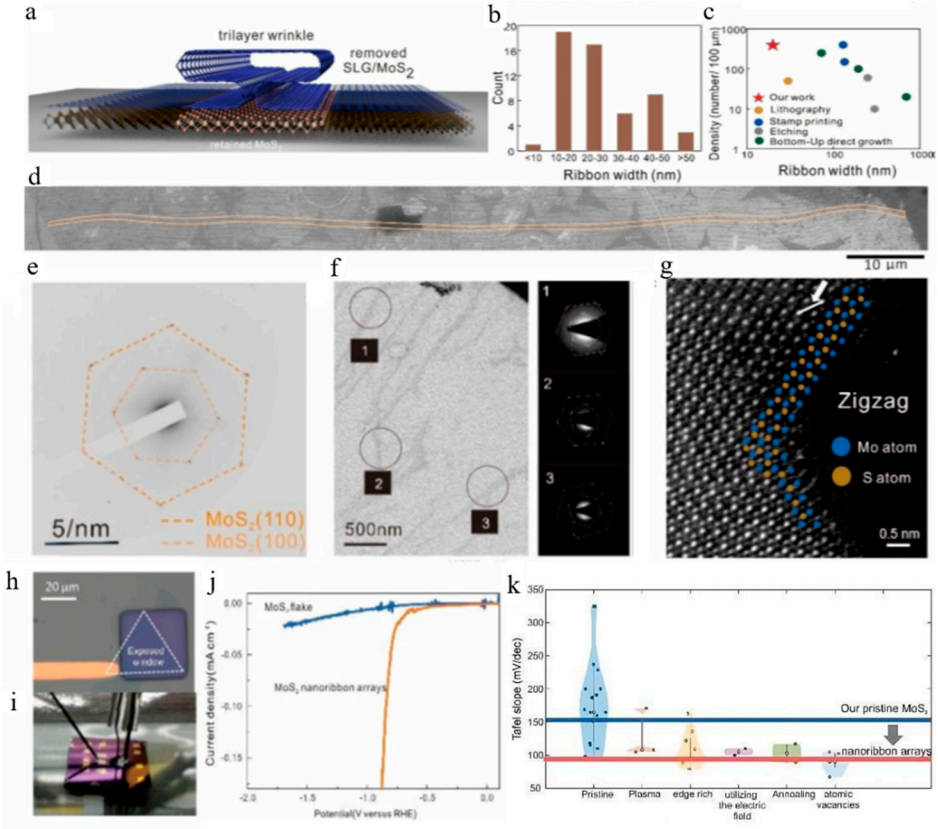

Figure 1. (**a**) Schematic representation of the wrinkle-templated nanoribbon formation. (**b**) A histogram which depicts the width distribution of nanoribbons was determined through analysis of transmission electron images. (**c**) A comparison between the attainable width and array density of nanoribbons in this study and previous results. (**d**) Composite SEM image with a nanoribbon exceeds 100μm. (**e**) A selected area diffraction pattern that indicates the symmetry of MoS_2. (**f**) A low resolution TEM image with SAED patterns demonstrates that three distinct areas exhibit long-range atomic alignment. (**g**) An atomic-resolution TEM image reveals the orientation of the lattice structure. (**h**) An optical micrograph displays a monolayer of 2H-MoS_2, showing an exposed reaction window and a gold contact. (**i**) A photograph illustrates the capillary microcell employed for HER measurements. (**j**) Comparing the performance of a MoS_2 flake and a nanoribbon array by polarization curves. (**k**) A comparative analysis between literature values of pristine and modified 2H-MoS_2 and the results obtained in this study. Adapted with permission from [53], Copyright 2023 Royal Society of Chemistry.

2.2. Fractal MoS_2

Since the catalytic active site of 2H-MoS_2 is mainly at its edge, controlling the morphology and structure of MoS_2 to expose more edges can further improve the hydrogen evolution reaction (HER) of MoS_2. Then, if MoS_2 is grown in a multi-branched and multi-edge morphology structure in the chemical vapor deposition (CVD) growth process, the HER performance of MoS_2 can be improved. Therefore, Yu G. et al. synthesized MoS_2 with different morphologies by adjusting the proportion of precursor in the process of MoS_2 generation by CVD.

As shown in Figure 2a,b, fractal MoS_2 and triangular MoS_2 were obtained by controlling the proportions of MoO_3 and S respectively, and the coverage rate of fractal MoS_2 and triangular MoS_2 was determined to be 20.5% and 22.7% by image analysis software. When MoO_3 is sufficient, a triangular MoS_2 can be generated, while at a low dose of MoO_3, a fractal MoS_2 will be generated. After the formation of MoS_2 with different morphologies, their catalytic properties were further evaluated. Figure 2c shows the polarization curves of the two MoS_2 samples, the GC electrode and Pt foil. Compared with triangular MoS_2, fractal MoS_2 has a smaller initial hydrogen evolution overpotential,

Preprints (www.preprints.org) | NOT PEER-REVIEWED | Posted: 17 August 2023 doi:10.20944/preprints202308.1283.v1

and as show in Figure 2d, The Tafel slope of fractal MoS_2 is lower than that of triangular MoS_2. It is confirmed that the fractal MoS_2 has more active edges and better catalytic activity.

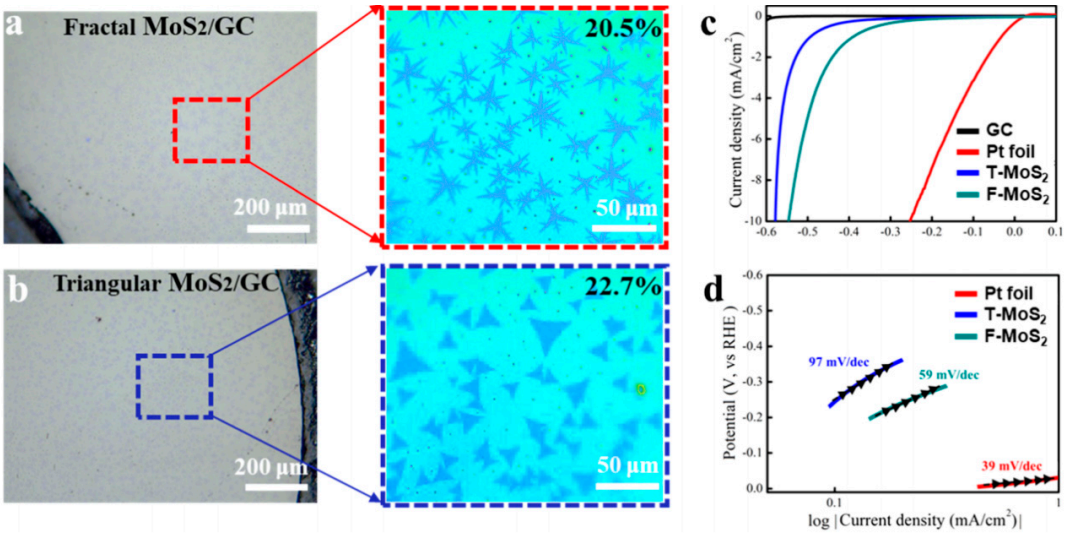

Figure 2. (**a, b**) Optic microscopy (OM) images of different kinds of MoS_2 transferred to the glassy carbon (GC) electrode, (**c**) polarization curves of the two MoS_2 samples, and (**d**) the Tafel slope diagram. Adapted with permission from [54], Copyright 2022 American Chemical Society.

3. Sulfur vacancies

Vacancies are considered to be the limiting doping states that promote atomic rearrangements and modulate the electronic structure over a wide range. There are many ways have been successfully implemented to introduce vacancies in 2D TMDs, such as hydrogen plasma exposure, H_2 annealing, Ar^{2+} beam irradiation, helium ion beam irradiation, showing great potential for catalytic reactions. However, all of the above methods require additional intervention from external stimuli, so it is a tough job to generate controllable vacancies directly by growth.

3.1. Salt-assisted chemical vapor deposition (CVD) method

Defect engineering is an effective strategy to accelerate the catalytic hydrogen production performance of MoS_2. However, introducing defects such as sulfur vacancies on MoS_2 basal plane is still a major challenge. Currently, sulfur vacancies are mainly introduced into MoS_2 by post-treatment methods such as plasma treatment, ultrasonic, ball milling and other methods. However, if sulfur vacancies can be introduced directly during the preparation of MoS_2, it would be an excellent strategy to prepare sulfur vacancy defects.

Preprints (www.preprints.org) | NOT PEER-REVIEWED | Posted: 17 August 2023 doi:10.20944/preprints202308.1283.v1

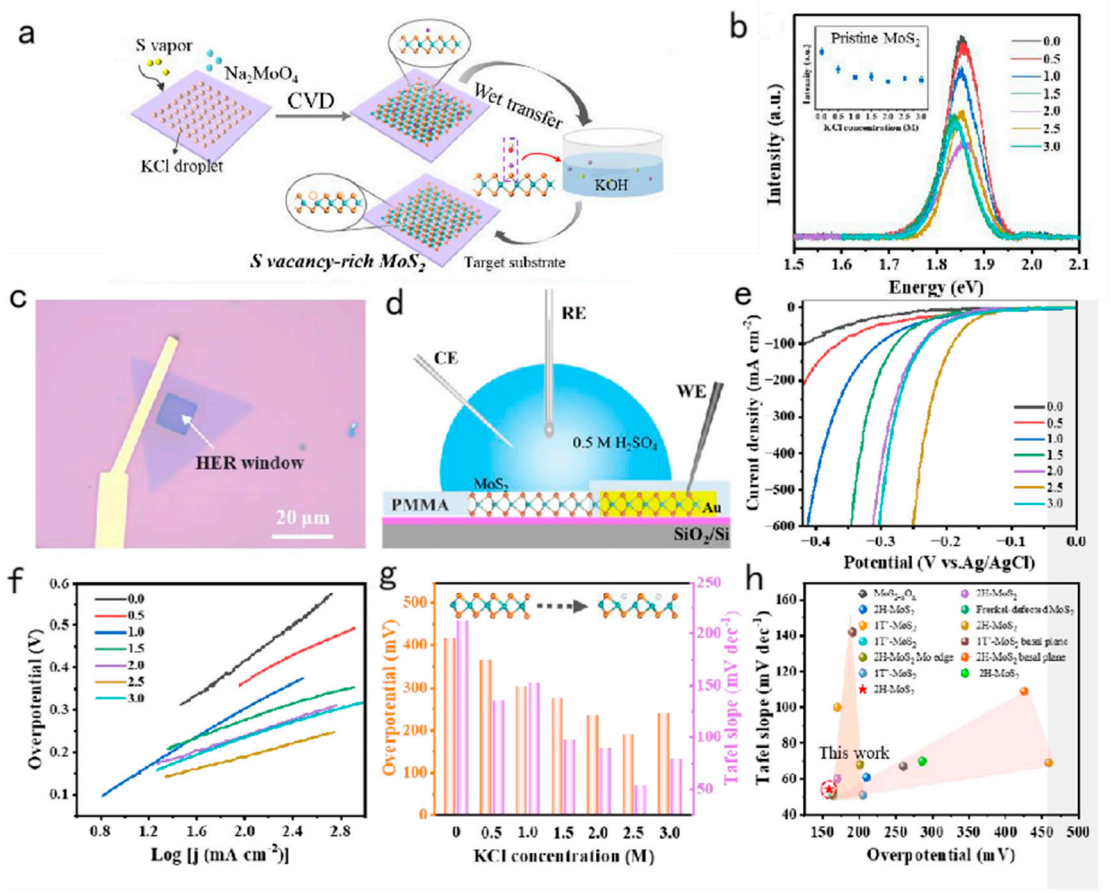

Figure 3. (**a**) Schematic illustration of the CVD growth of vacancy-rich MoS_2. (**b**) spectra of MoS_2 basal plane under various KCl concentration from 0.0 to 3.0 M. The inset shows the statistic results of PL intensity under each concentration (C_{KCl}). (**c**) optical image and (**d**) Schematic of the as-fabricated MoS_2 microdevice. WE: work electrode, RE: reference electrode, CE: counter electrode. (**e**) LSV curves and corresponding (**f**) Tafel plots of the MoS_2-KCl microdevices. (**g**) Comparison of overpotentials (red) and Tafel slopes (orange) under different KCl concentration. (**h**) The comparison of Tafel slope and overpotential of this work and reported MoS_2-based catalysts. Adapted with permission from [55], Copyright 202.

As shown in Figure 1a, Man et al. proposed that sulfur vacancies can be introduced into MoS_2 basal plane by controlling the reaction conditions during the MoS_2 growth through a salt-assisted CVD method. The density of sulfur vacancies could be controllable by controlling the added amount of KCl during the CVD growth process, and some kind of change has occurred in the process. Figure 1b shows that the luminescence spectra of the obtained MoS_2 with different density of sulfur vacancies, and it was found that the luminescence intensities of the obtained samples were different when the added amount of KCl is different, which indicates that the density of sulfur vacancies is positive correlation with the added amount of KCl. It is noted that energy band hold steady when added KCl reach a certain amount. The density of sulfur vacancies could be successfully controlled by this salt-assisted CVD method. In order to explore the relationship between the density of sulfur vacancies and the catalytic hydrogen production performance of MoS_2, micro-nano HER test platform was built in Figure 1c and d to precisely evaluate the catalytic performance of monolithic MoS_2 with sulfur vacancies. It was found that the samples with abundant sulfur vacancies had the best catalytic hydrogen production performance and the lowest Tafel slope (Figure 1e,f). The overpotential was negative correlation with the concentration of added KCl (Figure 1g), which confirmed that the sulfur vacancies of MoS_2 could be active sites for catalytic hydrogen production. The catalytic hydrogen production performance become much better when the density of sulfur vacancies is higher. Figure 1h shows the relationship between the overpotential and Tafel slope of all the samples with sulfur

 doi:10.20944/preprints202308.1283.v1

vacancy as reported in other literature. It could be seen that the sample obtained by this work has the best catalytic performance, which indicated salt-assisted CVD method is an excellent strategy to create the sulfur vacancies serving as HER catalytic active sites.

3.2. Controllable Thermochemical Generation of Active Defects

The method of thermochemical annealing sodium hypophosphite to produce MoS_2 active defects is proposed, meanwhile it can spontaneously produce PH_3 to regulate the MoS_2 lattice. By controlling the reaction conditions, active defects are formed at the basal plane and edges, thereby exposing more metal active sites and improving the Hydrogen Evolution Reaction (HER) performance of MoS_2. To develop efficient and low-cost MoS_2 catalysts for practical applications is important. Sodium hypophosphate is set around 200 °C to produce PH_3 gas, and MoS_2 is annealed by PH_3 gas at 500 °C as shown in Figure 4a. PH_3 will react with MoS_2 to produce defects that replace the S atom in the MoS_2 lattice through defects, resulting in P doping **(**Figure 4b**)**. Due to the active chemical properties of doped P, the active P element can be oxidized to a phosphate layer coating on the surface of MoS_2 and form phosphate without phosphate compounds in the MoS_2 crystal. The phosphate could be eventually removed from the crystal lattice of the MoS_2 crystal if it is dissolved in water or acid solution, thus creating defects again. Active defects may provide additional adsorption sites or change the local environment of the atom. When the proton is adsorbed to active defects from a relatively stable state, the ΔGH* (Gibbs free energy) of the system will change to regulate the thermodynamic adsorption/desorption of the proton. Energy level inhomogeneity can also be introduced to regulate the interface energy level and facilitate electron transport, which ultimately optimize HER activity **(**Figure 4c**)**. To further explore the more important factors for affecting HER activity, a microelectrochemical reactor was used to distinguish the influence of interfacial charge injection and thermodynamic adsorption, as shown in the schematic is the cross-section of monolayer graphene and PH_3 treated monolayer MoS_2 electrochemical device **(**Figure 4d**)**. The performance of single MoS_2 rather than the whole catalyst can be directly investigated in a microelectrochemical reactor, and the enhanced HER activity due to specific factors can be demonstrated. Graphene and unannealed/annealed MoS_2 monolayer nanosheets were prepared as contact electrodes and target catalysts, respectively. Comparing the relative overpotential of the four devices, it was found that the overpotential of the graphene-pMoS_2 heterostructure device was -100 mV at 10 $mA \cdot cm^{-2}$, which was much smaller than that of the other three devices, and the Tafel slope gradually decreased from curve 4 to 1 **(**Figure 4e**)**. The difference of curves in overpotential caused by charge transfer for 3 to 4 is -32 mV, while 1 to 2 is -60 mV. The thermodynamic ΔG_H^* is -140 mV for 1 to 3 and -112 mV for 2 to 4. It can be concluded from the data that charge transfer plays a less important role than thermodynamic ΔG_H^* due to drastic changes in properties.

Preprints (www.preprints.org) | NOT PEER-REVIEWED | Posted: 17 August 2023 doi:10.20944/preprints202308.1283.v1

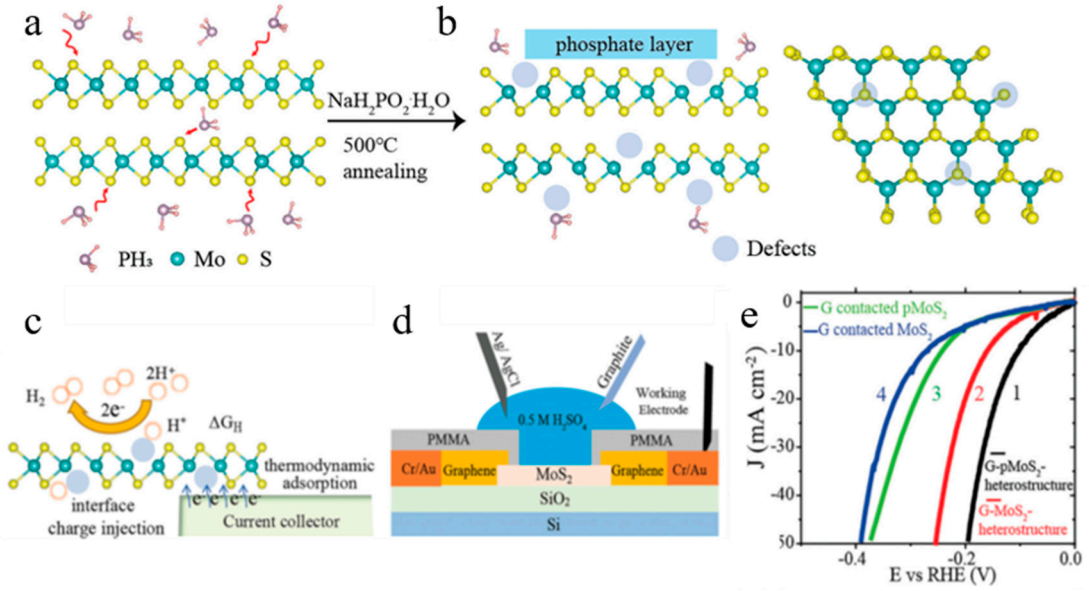

Figure 4. (**a**) Schematic of PH_3 molecule extracting sulfur atoms from the MoS_2 layers. (**b**) The defects formation in the basal planes, point/line defects, and edges, resulting in a H_3PO_4 layers on top of MoS_2 catalysts. (**c**) Schematic comparison of thermodynamic hydrogen adsorption and interface charge injection that determined the performance of hydrogen evolution reaction. (**d**) Schematic cross-section view of monolayer graphene and PH_3 treated monolayer MoS_2 electrochemical device. (**e**) Normalized polarization curves measured from different graphene and MoS_2 devices. Adapted with permission from [56], Copyright 2023 Wiley-VCH GmbH.

4. Phase

It is generally believed that the base plane of MoS_2 is inert, but it has been reported that the inert base plane can undergo a transient phase transition in the catalytic process to play the catalytic role, which is contrary to the common understanding that the catalytic activity is only at the edge. The HER catalytic mechanism of 1T-MoS_2 remains elusive and controversial. Therefore, it is necessary to further understand the mechanism of MoS_2 catalytic hydrogen production.

4.1. An Irreversible Phase Transition during Photocatalytic Hydrogen Evolution

It is widely believed the active sites of 2H-MoS_2 for catalytic hydrogen production are located at the edges, while its basal plane is inert. Then, it has been reported that the conversion of the 2H phase into the 1T phase by phase transformation is an ideal strategy to enhance the catalytic HER performance of MoS_2. However, the HER catalytic mechanism of 1T-MoS_2 remains elusive and controversial. It is hard to make clear the nature of the better catalytic performance, which is original form the improved electrical conductivity, the increased intrinsic activity of active site or the number of the active sites.

In order to explore this problem, Wang group make ultra-thin MoS_2 nanosheets vertically grown on TiO_2 nanofibers, and this vertical growth can introduce the strain. The 1T-MoS_2 with sulfur vacancies and strain could be obtained by further lithium intercalation. As shown in Figure 5a, using this sample as the catalyst for HER, it was found that its catalytic performance gradually increased during the process of catalytic hydrogen production. It was found that the catalytic hydrogen production per hour increased gradually with time in Figure 5b. This self-optimization of the catalytic performance is most likely due to the structural transformation of the catalyst during the catalytic HER process. In order to investigate this transformation, the catalyst after the catalytic reaction was structurally traced. The HRTEM in Figure 5c,d shown that the 1T phase has transformed into 1T′ phase with the super-lattice structure from Mo atom clustering into Zigzag chains. This suggests that

Preprints (www.preprints.org) | NOT PEER-REVIEWED | Posted: 17 August 2023 doi:10.20944/preprints202308.1283.v1

1T′ phase is the true active phase for catalytic HER. A molecular dynamics simulation was performed to research the transition from the 1T phase to the 1T′ phase (Figure 5e). It was found that the 1T phase with surface adsorbed hydrogen was more easily converted to the 1T′ phase, which means that the surface adsorbed hydrogen could promote the transformation of the 1T phase to the 1T′ phase. This is sufficient to show that in the photocatalytic HER process, the 1T phase with adsorbed hydrogen atoms on the surface could transform into the 1T′ phase with high activity, which leads to the phenomenon of self-optimization of the catalytic performance. This work well revealed the catalytic mechanism of 1T-phase MoS_2.

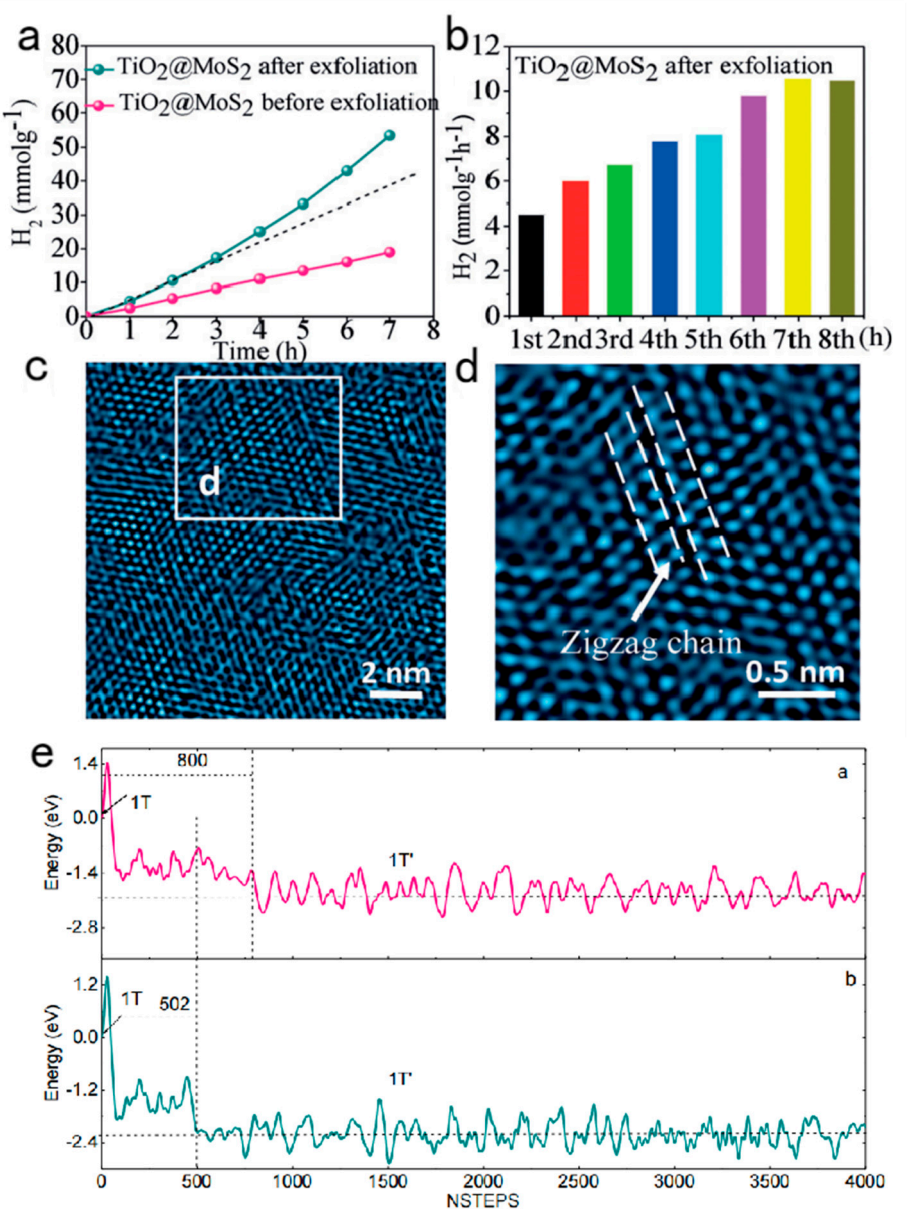

Figure 5. (**a**) H_2 accumulation and (**b**) H_2 production rate over exfoliated TiO_2@MoS_2 at each hour of the HER. All experiments were carried out in 80 mL of 15% (v/v) TEOA aqueous solution under visible light irradiation (λ>420 nm). Catalysts: 20 mg and EY: 20 mg. (**c**) HRTEM image of the MoS_2 in the exfoliated TiO_2@MoS_2 after 7 h HER. (**d**) Enlarged view of the square in c (the arrow points to the zigzag chain configuration of 1T′). (**e**) Evolution of total electronic energy by AIMD simulations in the MoS_2 phase transformation at 298 K. Adapted with permission from [13], Copyright 2017.

 doi:10.20944/preprints202308.1283.v1

4.2. Transient phase transition during the hydrogen evolution reaction

2H-MoS_2 is one of the most promising noble metal-free electrocatalysts in hydrogen evolution reaction (HER). With regard to its HER mechanism, the widely accepted view so far is that its marginal sites have high HER activity, while its basal plane is inert during HER process. However, Zhai et al. found that this conclusion was incorrect and verified it using ATR-SEIRAS and XAFS. The three-electrode ATR-SEIRAS cell used for in-situ measurement is shown in Figure 1a. As shown in Figure 1b, 0.5M H_2SO_4 was added to the three-electrode ATR-SEIRAS cell as the electrolyte, and the ATR-SEIRAS spectra of MoS_2 at -0.1 V, -0.2 V, -0.3 V and after reaction were measured. It can be found that a peak of 2523 cm^{-1} occurs at -0.2 V and -0.3 V and this peak is not from the edge site, but a continuous peak of 2600 cm^{-1} is from the edge site. The formation of S-H bond was observed at -0.2 V, indicating that 2523 cm^{-1} in the experiment is the stretching vibration of S-H bond (v(S-H)). Then, as shown in Figure 1d, the stretching vibration of S–H bond is calculated and compared with the experimental value. There are two adsorption modes of S-H bond in 2H-MoS_2, namely vertical adsorption and inclined adsorption. However, the calculated values of v(S-H) of the two models differ greatly from the experimental results. Similarly, the S-H bond in 1T′-MoS_2 also has two adsorption modes, which are respectively in the higher position and the lower position and are denoted as S-H and S-L. It is found that v(S-H) on S-L has a good agreement with the experimental value. In addition, as shown in Figure 1c,e, when the electrolyte H_2SO_4 in the experiment was replaced by D_2SO_4, that is, when the proton source in HER process was replaced by D, the conclusion remained unchanged, and v(S-H) on S-L also had a good agreement with the experimental value. The experimental results show that there is a phase transition from 2H to 1T′ during the reaction. As shown in Figure 1f–k, in order to further verify that the 2H to 1T′ phase transition is not permanent but transient, the EXAFS diagram during the reaction process and the wavelet transform analysis of 2H-MoS_2 are measured. As shown in Figure 1f, under OCP (open-circuit potential), the length of Mo-S bond and Mo-Mo bond is consistent with the those of 2H-MoS_2, while the length of Mo-Mo bond is consistent with 1T′-MoS_2 at -0.2 V and -0.3 V. It is found that the characteristics of 1T′-MoS_2 disappear after the end of the reaction, indicating that this phase transition is transient. As shown in Figure 1g–k, the WT data further indicates that this phase transition is transient, no 1T′-MoS_2 feature appears at OCP and -0.1 V, and 1T′ -MoS_2 feature appears at -0.2 V, and this feature is more obvious at -0.3 V, and when the reaction ends, the feature of 1T′-MoS_2 disappears. In conclusion, Zhai et al. verified that part of the base phase of 2H-MoS_2 would change into 1T′-MoS_2 during HER process, showing high activity, and 1T′-MoS_2 would change into 2H-MoS_2 after the reaction.

Preprints (www.preprints.org) | NOT PEER-REVIEWED | Posted: 17 August 2023 doi:10.20944/preprints202308.1283.v1

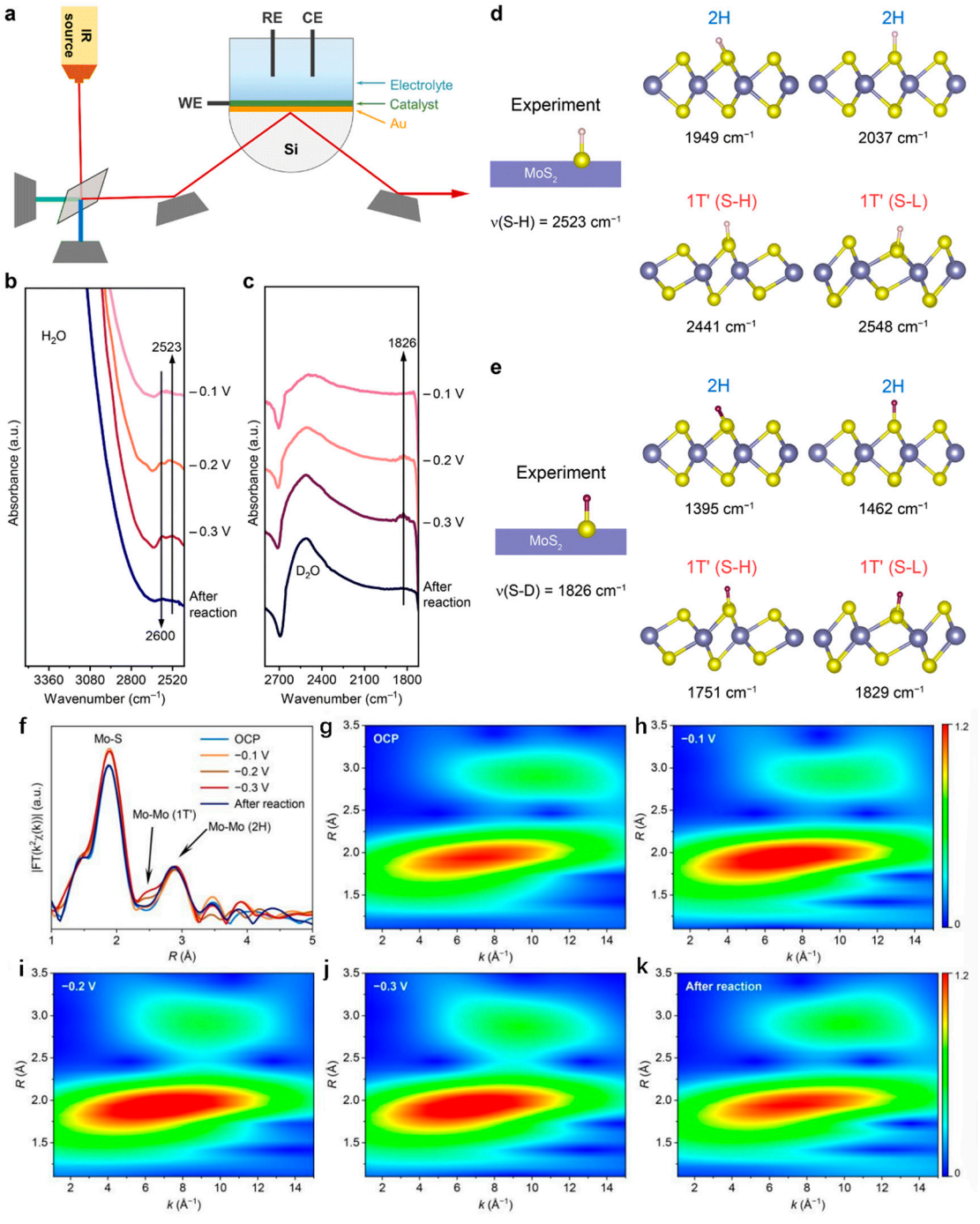

Figure 6. (**a**) Schematic diagram of a three-electrode ATR-SEIRAS cell measured in situ. (**b**) ATR-SEIRAS spectra of -0.1 V, -0.2 V, -0.3 V, and after the reaction measured in 0.5 M H_2SO_4 electrolyte and (**c**) 0.5 M D_2SO_4 electrolytes. (**d**) Comparison of ν(S-H) experimental data and calculated data of 2H-MoS_2 and 1T′-MoS_2. (**e**) Comparison of experimental and calculated data of ν(S-D) of 2H-MoS_2 and 1T′-MoS_2 after electrolyte replacement. The S atom is divided into S-H and S-L according to its position on 1T′-MoS_2. (**f**) In situ EXAFS spectra of 2H-MoS_2 with respect to reversible hydrogen electrodes (RHE) at OCP, -0.1 V, -0.2 V, and -0.3 V and after reaction. (**g-k**) Wavelet transform (WT) analysis of 2H-MoS_2 at (**g**) OCP, (**h**) at −0.1 V, (**i**) at −0.2 V, (**j**) at −0.3 V, and (**k**) after the reaction. Adapted with permission from [57], Copyright 2023 Royal Society of Chemistry.

5. Conclusion and outlook

A number of strategies have been developed to improve the catalytic production performance of MoS_2, and the mechanism of MoS_2 catalytic hydrogen production has also been proposed. It is very

necessary to summarize and re-understand the latest mechanism of catalytic hydrogen production. In this review, we summarized the latest strategies to improve the catalytic hydrogen production of MoS_2 and the mechanism of catalytic performance improvement. We believe that in this research field, it is necessary to further promote the improvement of MoS_2 catalytic hydrogen production performance from the following aspects. The catalyst with ideal atomic structure should be prepared in view of the controversy over the mechanism of MoS_2 catalytic hydrogen production, and the catalyst should be used as a model to explore the mechanism of catalytic hydrogen production, combined with first-principles calculation and in-situ characterization methods. The catalytic hydrogen production performance of MoS_2 should be standardized by constructing a micro-nano structure device, and the catalytic hydrogen production performance should be attributed to the catalytic active site with specific atomic structure.

Author Contributions: All authors have contributed to the writing of this manuscript. All authors have read and agreed to the published version of the manuscript.

Funding: This work was financially supported by the Natural Science Foundation of China (51902101), the Youth Natural Science Foundation of Hunan Province (2021JJ540044), the Natural Science Foundation of Jiangsu Province (BK20201381), and the Science Foundation of Nanjing University of Posts and Telecommunications (NY219144).

Institutional Review Board Statement: Not applicable.

Informed Consent Statement: Not applicable.

Data Availability Statement: Not applicable.

Conflicts of Interest: The authors declare no conflict of interest.

References

1. Jaramillo, T.F.; Jørgensen, K.P.; Bonde, J.; Nielsen, J.H.; Horch, S.; Chorkendorff, I. Identification of active edge sites for electrochemical H_2 evolution from MoS_2 nanocatalysts. *Science* 2007, 317, 100–102.
2. Voiry, D.; Yang, J.; Chhowalla, M. Recent strategies for improving the catalytic activity of 2D TMD nanosheets toward the hydrogen evolution reaction. *Adv. Mater.* 2016, 28, 6197–6206.
3. Chang, C.; Wang, L.; Xie, L.; Zhao, W.; Liu, S.; Zhuang, Z.; Liu, S.; Li, J.; Liu, X.; Zhao, Q. Amorphous molybdenum sulfide and its Mo-S motifs: Structural characteristics, synthetic strategies, and comprehensive applications. *Nano Res.* 2022, 15, 8613–8635.
4. Greeley, J.; Jaramillo, T. F.; Bonde, J.; Chorkendorff, I.; Nørskov, J. K. Computational high-throughput screening of electrocatalytic materials for hydrogen evolution. *Nat. Mater.* 2006, 5, 909–913
5. Voiry, D.; Fullon, R.; Yang, J.; de Carvalho Castro e Silva, C.; Kappera, R.; Bozkurt, I.; Kaplan, D.; Lagos, M. J.; Batson, P. E.; Gupta, G. et al. The role of electronic coupling between substrate and 2D MoS_2 nanosheets in electrocatalytic production of hydrogen. *Nat. Mater.* 2016, 15, 1003–1009.
6. Li, H.; Tsai, C.; Koh, A. L.; Cai, L. L.; Contryman, A. W.; Fragapane, A. H.; Zhao, J. H.; Han, H. S.; Manoharan, H. C.; Abild-Pedersen, F. et al. Activating and optimizing MoS_2 basal planes for hydrogen evolution through the formation of strained sulphur vacancies. *Nat. Mater.* 2016, 15, 48–53
7. Lin, L. X.; Sherrell, P.; Liu, Y. Q.; Lei, W.; Zhang, S. W.; Zhang, H. J.; Wallace, G. G.; Chen, J. Engineered 2D transition metal dichalcogenides—A vision of viable hydrogen evolution reaction catalysis. *Adv. Energy Mater.* 2020, 10, 1903870
8. Sun, C.; Wang, L.; Zhao, W.; Xie, L.; Wang, J.; Li, J.; Li, B.; Liu, S.; Zhuang, Z.; Zhao, Q. Atomic-Level Design of Active Site on Two-Dimensional MoS_2 toward Efficient Hydrogen Evolution: Experiment, Theory, and Artificial Intelligence Modelling. *Adv. Funct. Mater.* 2022, 2206163.
9. Lu, Q. P.; Yu, Y. F.; Ma, Q. L.; Chen, B.; Zhang, H. 2D transitionmetal-dichalcogenide-nanosheet-based composites for photocatalytic and electrocatalytic hydrogen evolution reactions. *Adv. Mater.* 2016, 28, 1917–1933.
10. He, Q.; Wang, L.; Yin, K.; Luo, S. Vertically aligned ultrathin 1T-WS_2 nanosheets enhanced the electrocatalytic hydrogen evolution. *Nanoscale Res. Lett.* 2018, 13, 167.
11. Chen, J.; Tang, Y.; Wang, S.; Xie, L.; Chang, C.; Cheng, X.; Liu, M.; Wang, L.; Wang, L. Ingeniously designed Ni-Mo-S/$ZnIn_2S_4$ composite for multi-photocatalytic reaction systems. *Chin. Chem. Lett.* 2022, 33, 1468–1474.
12. Wang, H. T.; Lu, Z. Y.; Kong, D. S.; Sun, J.; Hymel, T. M.; Cui, Y. Electrochemical tuning of MoS_2 nanoparticles on three-dimensional substrate for efficient hydrogen evolution. *ACS Nano* 2014, 8, 4940–4947

13. Wang, L.; Liu, X.; Luo, J.; Duan, X.; Crittenden, J.; Liu, C.; Zhang, S.; Pei, Y.; Zeng, Y.; Duan, X. Self-optimization of the active site of molybdenum disulfide by an irreversible phase transition during photocatalytic hydrogen evolution. *Angew. Chem.* 2017, 129, 7718–7722
14. Wang, H. T.; Lu, Z. Y.; Xu, S. C.; Kong, D. S.; Cha, J. J.; Zheng, G. Y.; Hsu, P. C.; Yan, K.; Bradshaw, D.; Prinz, F. B. et al. Electrochemical tuning of vertically aligned MoS_2 nanofilms and its application in improving hydrogen evolution reaction. *Proc. Natl. Acad. Sci.* USA 2013, 110, 19701–19706
15. Jiao, Y.; Zheng, Y.; Jaroniec, M.; Qiao, S. Z. Design of electrocatalysts for oxygen- and hydrogen-involving energy conversion reactions. *Chem. Soc. Rev.* 2015, 44, 2060–2086.
16. Zou, X. X.; Zhang, Y. Noble metal-free hydrogen evolution catalysts for water splitting. *Chem. Soc. Rev.* 2015, 44, 5148–5180.
17. Yu, Y. F.; Huang, S. Y.; Li, Y. P.; Steinmann, S. N.; Yang, W. T.; Cao, L. Y. Layer-dependent electrocatalysis of MoS_2 for hydrogen evolution. *Nano Lett.* 2014, 14, 553–558.
18. Zhang, J.; Hong, H.; Lian, C.; Ma, W.; Xu, X. Z.; Zhou, X.; Fu, H. X.; Liu, K. H.; Meng, S. Interlayer-state-coupling dependent ultrafast charge transfer in MoS_2 /WS_2 bilayers. *Adv. Sci.* 2017, 4, 1700086.
19. Ji, Z. H.; Hong, H.; Zhang, J.; Zhang, Q.; Huang, W.; Cao, T.; Qiao, R. X.; Liu, C.; Liang, J.; Jin, C. H. et al. Robust stacking-independent ultrafast charge transfer in MoS_2 /WS_2 bilayers. *ACS Nano* 2017, 11, 12020–12026.
20. Wang, L.; Shih, E. M.; Ghiotto, A.; Xian, L. D.; Rhodes, D. A.; Tan, C.; Claassen, M.; Kennes, D. M.; Bai, Y. S.; Kim, B. et al. Correlated electronic phases in twisted bilayer transition metal dichalcogenides. *Nat. Mater.* 2020, 19, 861–866.
21. Li, Y.; Wang, L.; Cai, T.; Zhang, S.; Liu, Y.; Song, Y.; Dong, X.; Hu, L. Glucose-assisted synthesize 1D/2D nearly vertical CdS/MoS_2 heterostructures for efficient photocatalytic hydrogen evolution. *Chem. Eng. J.* 2017, 321, 366–374.
22. Liu, C.; Wang, L.; Tang, Y.; Luo, S.; Liu, Y.; Zhang, S.; Zeng, Y.; Xu, Y. Vertical single or few-layer MoS_2 nanosheets rooting into TiO_2 nanofibers for highly efficient photocatalytic hydrogen evolution. *Appl. Catal. B* 2015, 164, 1–9.
23. Li, Y.; Yin, K.; Wang, L.; Lu, X.; Zhang, Y.; Liu, Y.; Yan, D.; Song, Y.; Luo, S. Engineering MoS_2 nanomesh with holes and lattice defects for highly active hydrogen evolution reaction. *Appl. Catal. B* 2018, 239, 537–544.
24. Li, Y.; Yu, B.; Li, H.M.; Liu, B.; Yu, X.; Zhang, K.W.; Qin, G.; Lu, J.H.; Zhang, L.H.; Wang, L.L. Activation of hydrogen peroxide by molybdenum disulfide as Fenton-like catalyst and cocatalyst: Phase-dependent catalytic performance and degradation mechanism. *Chin. Chem. Lett.* 2023, 34, 107874.
25. Li, J.W.; Yin, W.N.; Pan, J.A.; Zhang, Y.B.; Wang, F.S.; Wang, L.L.; Zhao, Q. External field assisted hydrogen evolution reaction. *Nano Res.* 2023,16, 8638–8654.
26. Wang, L.; Liu, X.; Zhang, Q.; Zhou, G.; Pei, Y.; Chen, S.; Wang, J.; Rao, A.; Yang, H.; Lu, B. Quasi-one-dimensional Mo chains for efficient hydrogen evolution reaction. *Nano Energy* 2019, 61, 194–200.
27. Wang, S.; Wang, L.; Xie, L.; Zhao, W.; Liu, X.; Zhuang, Z.; Zhuang, Y.; Chen, J.; Liu, S.; Zhao, Q. Dislocation-strained MoS_2 nanosheets for high-efficiency hydrogen evolution reaction. *Nano Res.* 2022, 15, 4996–5003.
28. Xie, L.; Wang, L.; Zhao, W.; Liu, S.; Huang, W.; Zhao, Q. WS_2 moire superlattices derived from mechanical flexibility for hydrogen evolution reaction. *Nat. Commun.* 2021, 12, 5070.
29. Liu, M.; Li, H.; Liu, S.; Wang, L.; Xie, L.; Zhuang, Z.; Sun, C.; Wang, J.; Tang, M.; Sun, S.; et al. Tailoring activation sites of metastable distorted 1T′ -phase MoS_2 by Ni doping for enhanced hydrogen evolution. *Nano Res.* 2022, 15, 5946–5952.
30. Park, S.; Park, J.; Abroshan, H.; Zhang, L.; Kim, J. K.; Zhang, J. M.; Guo, J. H.; Siahrostami, S.; Zheng, X. L. Enhancing catalytic activity of MoS_2 basal plane S-vacancy by Co cluster addition. *ACS Energy Lett.* 2018, 3, 2685–2693.
31. Mahler, B.; Hoepfner, V.; Liao, K.; Ozin, G. A. Colloidal synthesis of 1T-WS_2 and 2H-WS_2 nanosheets: Applications for photocatalytic hydrogen evolution. *J. Am. Chem. Soc.* 2014, 136, 14121–14127.
32. Yin, Y.; Zhang, Y. M.; Gao, T. L.; Yao, T.; Zhang, X. H.; Han, J. C.; Wang, X. J.; Zhang, Z. H.; Xu, P.; Zhang, P. et al. Synergistic phase and disorder engineering in 1T-$MoSe_2$ nanosheets for enhanced hydrogen-evolution reaction. *Adv. Mater.* 2017, 29, 1700311.
33. Voiry, D.; Yamaguchi, H.; Li, J. W.; Silva, R.; Alves, D. C. B.; Fujita, T.; Chen, M. W.; Asefa, T.; Shenoy, V. B.; Eda, G. et al. Enhanced catalytic activity in strained chemically exfoliated WS_2 nanosheets for hydrogen evolution. Nat. Mater. 2013, 12, 850–855.
34. Tan, C. L.; Luo, Z. M.; Chaturvedi, A.; Cai, Y. Q.; Du, Y. H.; Gong, Y.; Huang, Y.; Lai, Z. C.; Zhang, X.; Zheng, L. R. et al. Preparation of high-percentage 1T-phase transition metal dichalcogenide nanodots for electrochemical hydrogen evolution. *Adv. Mater.* 2018, 30, 1705509
35. Wang, L.; Xie, L.; Zhao, W.; Liu, S.; Zhao, Q. Oxygen-facilitated dynamic active-site generation on strained MoS_2 during photo-catalytic hydrogen evolution. *Chem. Eng. J.* 2021, 405, 127028.

36. Guo, Y. B.; Chen, Q.; Nie, A. M.; Yang, H.; Wang, W. B.; Su, J. W.; Wang, S. Z.; Liu, Y. W.; Wang, S.; Li, H. Q. et al. 2D hybrid superlattice-based on-chip electrocatalytic microdevice for in situ revealing enhanced catalytic activity. *ACS Nano* 2020, 14, 1635–1644.

37. Chou, S. S.; Sai, N.; Lu, P.; Coker, E. N.; Liu, S.; Artyushkova, K.; Luk, T. S.; Kaehr, B.; Brinker, C. J. Understanding catalysis in a multiphasic two-dimensional transition metal dichalcogenide. *Nat. Commun.* 2015, 6, 8311.

38. Jin, H. Y.; Liu, X.; Chen, S. M.; Vasileff, A.; Li, L. Q.; Jiao, Y.; Song, L.; Zheng, Y.; Qiao, S. Z. Heteroatom-doped transition metal electrocatalysts for hydrogen evolution reaction. *ACS Energy Lett.* 2019, 4, 805–810

39. Wang, L.; Zhou, G.; Luo, H.; Zhang, Q.; Wang, J.; Zhao, C.; Rao, A.; Xu, B.; Lu, B. Enhancing catalytic activity of tungsten disulfide through topology. *Appl. Catal. B* 2019, 256, 117802.

40. Wang, L.; Duan, X.; Wang, G.; Liu, C.; Luo, S.; Zhang, S.; Zeng, Y.; Xu, Y.; Liu, Y.; Duan, X. Omnidirectional enhancement of photocatalytic hydrogen evolution over hierarchical "cauline leaf" nanoarchitectures. *Appl. Catal. B* 2016, 186, 88–96.

41. Li, M.Z.; Wang, L.L.; Zhang, X.Y.; Yin, W.A.; Zhang, Y.B.; Li, J.W.; Yin, Z.Y.; Cai, Y.T.; Liu, S.J.; Zhao, Q. Recent status and future perspectives of $ZnIn_2S_4$ for energy conversion and environmental remediation. *Chin. Chem. Lett.* 2023, 34, 107775.

42. Li, Y.; Hua, Y.Q.; Sun, N.; Liu, S.J.; Li, H.X.; Wang, C.; Yang, X.Y.; Zhuang, Z.C.; Wang, L.L. Moire superlattice engineering of two-dimensional materials for electrocatalytic hydrogen evolution reaction. *Nano Res.* 2023, 16, 8712–8728

43. Xu, Y.; Wang, L.; Liu, X.; Zhang, S.; Liu, C.; Yan, D.; Zeng, Y.; Pei, Y.; Liu, Y.; Luo, S. Monolayer MoS_2 with S vacancies from interlayer spacing expanded counterparts for highly efficient electrochemical hydrogen production. *J. Mater. Chem. A Mater.* 2016, 4, 16524–16530.

44. Ye, G. L.; Gong, Y. J.; Lin, J. H.; Li, B.; He, Y. M.; Pantelides, S. T.; Zhou, W.; Vajtai, R.; Ajayan, P. M. Defects engineered monolayer MoS_2 for improved hydrogen evolution reaction. *Nano Lett.* 2016, 16, 1097–1103.

45. Wang, L.; Shih, E. M.; Ghiotto, A.; Xian, L. D.; Rhodes, D. A.; Tan, C.; Claassen, M.; Kennes, D. M.; Bai, Y. S.; Kim, B. et al. Correlated electronic phases in twisted bilayer transition metal dichalcogenides. *Nat. Mater.* 2020, 19, 861–866.

46. Yuan, Y.; Pan, J., Yin; W., Yu, H.; Wang, F.; Hu, W.; Yan, D.; Wang, L. Effective strategies to promote Z (S)-scheme photocatalytic water splitting. *Chin. Chem. Lett.* 2023, 108724.

47. Yin, W.; Yuan, L.; Huang, H.; Cai, Y.; Pan, J.; Sun, N.; Zhang, Q.; Shu, Q.; Gu, C.; Zhuang, Z.; Wang, L. Strategies to accelerate bubble detachment for efficient hydrogen evolution. *Chin. Chem. Lett.* 2023, 108351.

48. Yu, H.; Zhang, M.; Cai, Y., Zhuang Y.; Wang, L. The Advanced Progress of MoS_2 and WS_2 for Multi-Catalytic Hydrogen Evolution Reaction Systems. *Catalysts*. 2023, *13*(8), 1148.

49. Zhang, Y.; Pan, J.; Gong, G.; Song, R.; Yuan, Y.; Li, M.; Wang, L. In Situ Surface Reconstruction of Catalysts for Enhanced Hydrogen Evolution. *Catalysts*, 2023, *13*(1), 120.

50. Fan, P.; He, Y.; Pan, J.; Sun, N.; Zhang, Q.; Gu, C.; Chen, K.; Yin, W.; Wang, L. Recent advances in photothermal effects for hydrogen evolution. *Chin. Chem. Lett.* 2023, 108513.

51. Yin, Z.; Xie, L.; Yin, W.; Zhi, T.; Chen, K.; Pan, J.; Zhang, Y.; Li, J.; Wang, L. Advanced development of grain boundaries in TMDs from fundamentals to hydrogen evolution application. *Chin. Chem. Lett.* 2023, 108628.

52. Li, M.; Yin, W.; Pan, J.; Zhu, Y.; Sun, N.; Zhang, X.; Wan, Y.; Luo, Z.; Yi, L.; Wang, L. Hydrogen spillover as a promising strategy for boosting heterogeneous catalysis and hydrogen storage. *Chem. Eng. J.*, 2023, 471, 144691.

53. Chen, D. R.; Muthu, J.; Guo, X. Y.; Chin, H. T.; Lin, Y. C.; Haider, G.; Ting, C.; Kalbáč, M.; Hofmann, M.; Hsieh, Y. P. Edge-dominated hydrogen evolution reactions in ultra-narrow MoS_2 nanoribbon arrays. *J. Mater. Chem. A.* 2023, DOI: 10.1039/D3TA01573D.

54. Wang, S.; Li, J.; Hu, S.; Kang, H.; Zhao, S.; Xiao, R.; Sui, Y; Chen, Z; Peng, S.; Jin, Z.; Liu, X; Zhang Y.; Yu, G. Morphology Regulation of MoS_2 Nanosheet-Based Domain Boundaries for the Hydrogen Evolution Reaction. *ACS Appl. Nano Mater.*, 2022, *5*, 2273-2279.

55. Man, P.; Jiang, S.; Leung, K. H.; Lai, K. H.; Guang, Z.; Chen, H.; Huang, L.; Chen, T.; Gao, S.; Peng, Y.; Lee, C.; Deng Q.; Zhao, J.; Ly, T. H. Salt-Induced High-Density Vacancy-Rich Two-Dimensional MoS_2 for Efficient Hydrogen Evolution. *Adv. Mater.*, 2023, 2304808.

56. Zhou, Y.; Li, C.; Zhang, Y.; Wang, L.; Fan, X.; Zou, L.; Cai, Z., Jiang J.; Zhou, S.; Zhang, B.; Li, W.; Chen, Z. Controllable Thermochemical Generation of Active Defects in the Horizontal/Vertical MoS_2 for Enhanced Hydrogen Evolution. *Adv. Funct. Mater.*, 2023, 2304302.

57. Zhao, Y.; Li, H.; Yang, R.; Xie, S.; Liu, T.; Li, P.; Zhai, T. Transient phase transition during the hydrogen evolution reaction. *Energy Environ. Sci.*, 2023, DOI: 10.1039/D3EE01409F.